Voltage stability in a grid-connected inverter with automatic Volt-Watt and Volt-VAR functions

Julio H. Braslavsky, *Senior Member, IEEE*, Lyle D. Collins, and John K. Ward, *Member, IEEE*

***Abstract*—The growing uptake of solar power in low-voltage grids across the world has drawn attention to potential overvoltage issues. In an effort to mitigate overvoltage, automatic Volt-Watt and Volt-VAR inverter response functions have been introduced in recent standards. The utility of these functions has been established in a number of recent studies. However, relatively little analysis exists on the stability of grid-connected inverters where decentralised operation of these response functions can potentially trigger undesirable interactions. This paper presents a rigorous stability analysis of a grid-connected inverter under simultaneous operation of automatic Volt-Watt and Volt-VAR response functions. Conditions for the existence of an equilibrium voltage are established together with tests that characterise its stability in terms of the inverter and line parameters. The analysis reveals a little-known stability vulnerability arising when both Volt-Watt and Volt-VAR functions are in operation if Watt output takes precedence over the provision of VAR support, a generally recommended setting. To circumvent this vulnerability, the proposed stability tests allow parameter selection for guaranteed stability margins. A safe configuration alternative is also identified to avoid instability at the expense of real power output. Numerical methods to compute equilibrium voltages are presented and used in two illustrative numerical studies.**

***Index Terms*—Stability analysis; Stability criteria; Reactive power control; Photovoltaic power systems; Voltage control; DC-AC power conversion; Power quality; Power distribution control; Overvoltage protection; Distributed control; Current-controlled inverters.**

I. Introduction

A. The emergence of inverters with grid-support functions

Dramatic reductions in costs have promoted the development of renewable energy technologies even in the absence of capital subsidies and in a context of lower fossil fuel prices. Solar energy generated from photovoltaic (PV) panels is an increasingly critical part of the energy supply. Germany leads the way with an installed PV capacity that already exceeds that of all other types of power plants and covers approximately 7.5% of the country's net energy electricity consumption. More than 98% of Germany's over one million PV power plants are connected to low-voltage grids, and 75% of them have an installed capacity below 1 MW [1]. In other countries, directed incentives towards small-scale PV systems have resulted in even more distributed decentralised PV generation. Australia, for example, has over 1.6 million small-scale PV systems with an aggregate installed capacity already exceeding 10% of the peak electricity demand of the primary electricity grid; 98% of these systems have an installed capacity below 10kW [2], [3].

PV systems are connected to the grid via an inverter, which converts electricity generated by the PV panels as a direct current into a grid-compatible alternating current. Depending on the inverter output, the inverter can be current-controlled if the output is controlled to appear to the grid as a current source and voltage-controlled if the output is controlled to appear to the grid as a voltage source. Current-controlled inverters are easier to implement and are typically used to maximise PV power output exported to the grid [4].

However, high density distributed PV generation can be problematic, particularly with current-controlled inverters, which cannot directly contribute to the regulation of power system frequency and voltage [4, Chapter 18], with increased voltage swings and overvoltages (voltages exceeding design or regulated limits) a reported consequence [5, p. 75]. Voltage rise is likely to occur whenever generation exceeds consumption — the typical context being solar generation exceeding household load. Concerns about such voltage issues motivated electricity utilities in Australia to place precautionary restrictions on PV installations, such as limiting size, preventing energy exports to the grid, requiring specific reactive power or power factor settings, or limiting ramp rates [6], [7]. Ramp rate restrictions effectively require installations to include energy storage to minimise rapid fluctuations in power output such as those arising from passing clouds.

In a contrasting response to potential voltage swings and overvoltages, inverter manufacturers have developed new grid-support functions, such as Volt-Watt and Volt-VAR response functions, which allow the gradual curtailment of real power and/or the consumption of reactive power to mitigate overvoltages. The curtailment of real power through a Volt-Watt function improves asset utilisation over the earlier practice of simply shutting down the inverter in an overvoltage event. The inclusion of reactive power control through a Volt-VAR function can allow higher levels of real power output whilst still contributing to mitigate overvoltages. These functions have been advocated by the Electric Power Research Institute [8, §9,§10] and feature in current standards for grid-connected inverters [9]–[11]. Typical response shapes recommended are illustrated in Figure 1.

B. Existing research work

The utility of these new grid-support functions has been established in a number of recent studies [12]–[21]. How-

The authors are with the Commonwealth Scientific and Industrial Research Organisation (CSIRO), CSIRO Energy Centre, Mayfield West, NSW 2304, Australia

J. H. Braslavsky and L. D. Collins are also with the School of Electrical Engineering and Computing, The University of Newcastle, Australia

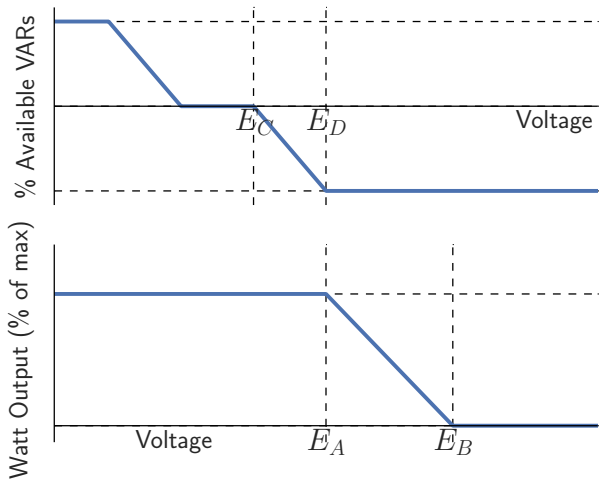

Fig. 1. The Volt-VAR support function (top) and the Volt-Watt constraint function (bottom)

ever, relatively little analysis exists on the stability of grid-connected inverters where the decentralised operation of such functions can potentially trigger undesirable interactions. A stability analysis in [13] of a grid-connected inverter with Volt-VAR response functionality shows that delay in the voltage measurement may lead to instability in the response. Similar instabilities are identified in a numerical study in [16], from which the authors derive empirical criteria for stability in terms of the system parameters for single and multi-inverter cases. Numerical simulations in [14, §4] show that instability may also arise when Volt-Watt and Volt-VAR functions are implemented simultaneously. The simulations in [14], [16] provide evidence that stability can critically depend on the line impedance and the voltage measurement filter.

The authors in [12] investigated the effectiveness of adjusting both Volt-Watt and Volt-VAR functions according to local network characteristics to maximise PV hosting capacity, which they demonstrate on a small experimental trial. Recent works [15], [19]–[21] also adopt combined Volt-Watt, Volt-VAR strategies to optimise voltage management capabilities of inverters by tuning the balance between active and reactive power responses to the characteristics of the local network.

Most of the existing stability analyses for inverters with active and reactive power response capabilities are based on numerical studies, while theoretically-based analyses are scarce. Of the theoretically-based existing stability work, the analysis in [13] is limited to inverters with a Volt-VAR response function and no power curtailment capabilities. A small-gain stability analysis is developed in the recent work [21]. The authors exploit the stability criterion developed to derive an interesting optimal control scheme with guaranteed input-output stable solutions. While the stability analysis in [21] addresses the case of multiple distributed inverters, it applies to a linear approximation of the system that is assumed to have a bounded error with respect to the exact nonlinear power flow equations. It is not clear how such approximation error could be quantified or guaranteed to be small, and hence the ensuing stability criterion may not capture sustained local voltage oscillations or other instabilities arising from nonlinear dynamic interactions.

The stability of inverters connected to low-voltage networks thus remains a challenging topical problem that requires further analysis and understanding. While the stability of generators connected to high and medium-voltage networks is well-understood [22], assumptions typically made to simplify the analysis in high-voltage lines (e.g., line impedance predominantly inductive) do not apply to low-voltage distribution networks, where small PV generators are increasingly prevalent.

C. Main contributions

The present paper extends the existing body of work by developing a rigorous stability analysis of a current-controlled inverter with Volt-VAR and Volt-Watt automatic response functions connected to a low-voltage network. The paper provides conditions for the existence of equilibria and analytic criteria for their stability. These criteria are used to characterise a previously unidentified stability vulnerability arising in the event of significant voltage rise whilst the inverter is operating at or near its real power output capacity. For the simple case of an inverter connected through a lossy line to the distribution network, it is shown that sustained voltage oscillations may be triggered when both Volt-Watt and Volt-VAR functions are in operation if the inverter Watt output takes precedence over the provision of VAR support. Without further analysis, such precedence may be taken as the generally preferred option to maximise PV power exported to the grid [8, pp. 10-6–10-8]. However, as shown in the present paper, with the Volt-VAR function designed to utilise as much of the available inverter capacity as possible, its activation in conjunction with the Volt-Watt function may result in sustained oscillations of voltage and power output. These potential oscillations were first identified and numerically verified by the authors in [23].

This paper makes the following main original contributions:

(a) a rigorous mathematical characterisation and proof for the existence of an equilibrium voltage when both the Volt-Watt and the Volt-VAR responses are in operation
(b) non-conservative tests for stability of the equilibrium voltage, which may be efficiently evaluated numerically
(c) parametric tests for stability that, at the expense of some conservatism, enable the direct design of parameter ranges for implementation with guaranteed stability margins.

In addition, the paper provides numerical procedures to compute voltage equilibria for any given set of inverter and line parameters. These procedures are implemented in two numerical studies that demonstrate stability and instability as predicted by the analysis developed, and a thorough comparison of the proposed theoretic and parametric tests for stability over a range of parameters for the voltage measurement filter and the line impedance.

The rest of the paper is organised as follows: Section II defines the system considered, assumptions, and underlying power and voltage relationships. Section III contains the main contributions of the paper: the mathematical framework (Section III-A), conditions for the existence of an equilibrium

voltage (Section III-B) and numerical procedures for its computation (Section III-C), and tests for stability (Section III-D). Stability implications are discussed in terms of the system parameters in Section III-E. Two illustrative numerical studies are presented in Section IV. The paper is summarised with concluding remarks in Section V.

II. Preliminaries

A. System definition

Consider the two-bus system illustrated in Figure 2, where a current-controlled inverter is connected to an external grid through a line impedance $z = R + jX = Z\angle\theta$. The inverter represents a single-phase, or a balanced three-phase device capable of delivering real power to the external grid with any power factor. The voltage at the inverter bus is denoted U, and the voltage at the grid bus is denoted V.

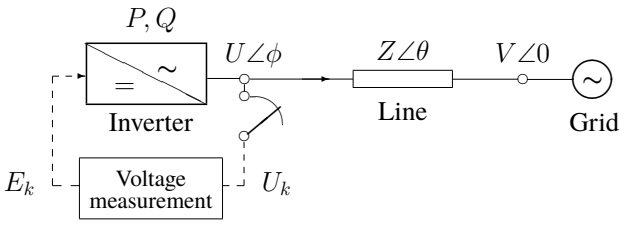

Fig. 2. Inverter connected to an infinite bus

The inverter is assumed to be exporting real power to the grid in a mode of operation where its active and reactive output powers are responsive to the inverter bus voltage U, which is available to the inverter as a sampled-data measurement E_k obtained as the output of a stable voltage measurement device.

The external grid is represented as an infinite bus assumed to regulate frequency and voltage, with $V\angle 0$ taken as the phase reference. The line impedance z is assumed to have non-zero resistance and is inductive so that both R and X are positive.

Current flowing from the inverter to the external grid is defined as positive, from which it follows that delivered real and reactive powers are defined as positive, in accordance with generator convention [24]. The term 'injection' is used to refer to the magnitude of the reactive power delivered/absorbed. The Volt-VAR function (specified in more detail below) indicates that reactive power is injected as voltage increases.

The voltage $U\angle\phi$ at the point of connection of the inverter to the line must satisfy, in steady-state, the nonlinear algebraic relationship with the injected powers, line impedance, and grid voltage, as given by the following fact.

Fact 1 (Voltage at inverter connection point)**.** *The voltage magnitude U at the connection point between the inverter and the external grid in the system illustrated in Figure 2 satisfies the steady-state algebraic equation*

$$U^4 - \big(2(RP + XQ) + V^2\big)U^2 + (P^2 + Q^2)Z^2 = 0. \quad (1)$$

Proof. The complex current injected by the power source is given by $I = (G + jB)\left(Ue^{j\phi} - V\right)$, where $G + jB = Y\angle -\theta = z^{-1}$ is the line admittance. The real and imaginary components of the apparent power $S = I^* E e^{j\phi}$ injected by the inverter into the grid satisfy the power-flow equations [22, § 6.4]

$$P = U^2 G - VU\left(G\cos\phi + B\sin\phi\right), \quad (2)$$

$$Q = -U^2 B - VU\left(G\sin\phi - B\cos\phi\right). \quad (3)$$

The sum of (2) multiplied by B and (3) multiplied by G is

$$PB + QG = -VUY^2\sin\phi, \quad (4)$$

and the difference between (2) multiplied by G and (3) multiplied by B is

$$PG - QB - U^2Y^2 = -VUY^2\cos\phi. \quad (5)$$

Squaring and adding (4) and (5) to eliminate $\cos\phi$ and $\sin\phi$ yields $U^4Y^4 - U^2Y^2\left(2\left(PG - QB\right) + V^2Y^2\right) + Y^2\left(P^2 + Q^2\right) = 0$, from which (1) follows by substituting $G = R/(R^2 + X^2)$ and $B = -X/(R^2 + X^2)$. □

For given values of P, Q, V, R, X, the equation (1) admits only two real positive solutions,. Namely, a high-voltage feasible solution U^+ and a low-voltage infeasible solution U^- [25], defined by

$$U^{\pm} = \Bigg[RP + XQ + {}^{V^2}\!/_2 \pm \Big[\left(RP + XQ + {}^{V^2}\!/_2\right)^2 - (P^2 + Q^2)Z^2\Big]^{1/2}\Bigg]^{1/2}. \quad (6)$$

Both solutions exist if the discriminant

$$\left(RP + XQ + {}^{V^2}\!/_2\right)^2 - (P^2 + Q^2)Z^2 \geq 0. \quad (7)$$

Expressions such as (6) have been used in line loadability studies (e.g. [26]). The analysis in the present paper focuses on the high-voltage feasible solution U^+.

B. Volt-Watt and Volt-VAR response functions

Following [8], [9], the inverter is equipped with Volt-Watt and Volt-VAR grid-support response functions as illustrated in Figure 1. The purpose of these functions is to trigger automatic absorption of reactive power and curtailment of active power in the event of overvoltage by calculating reference values for the inverter injected powers P and Q as functions of the measurement E_k of the voltage U_k at the inverter point of connection (see Figure 2), where E_k, U_k represent voltage magnitudes at the discrete-time instant k. In an ideal measurement $E_k = U_k$. However, as described in Section III, all dynamics arising in the Volt-Watt / Volt-VAR response feedback loops will be lumped in the dynamics of the measurement filter. Thus, in general $E_k \neq U_k$, except once an equilibrium is reached.

Curtailment of real power output with the Volt-Watt function $\mathcal{P}(E)$ is defined, following existing guidelines [8], [9], as

$$\mathcal{P}(E) = \begin{cases} \mu S[1 - d(E - E_A)] & \text{if } E \in [E_A, E_B] \\ \mu S[1 - d(E_B - E_A)] & \text{if } E > E_B, \end{cases} \quad (8)$$

where μ is a fractional measure of the real power output of the inverter relative to its maximum capacity $S > 0$ at the instant overvoltage occurs. The Volt-Watt response function (8) is configured by the real parameters d, E_A and E_B ($E_B >$

E_A), such that the lowest value to which real power output can be curtailed is nonnegative, namely

$$\mu S[1 - d(E_B - E_A)] \geq 0.$$

When the measured voltage is less than E_A, no constraints are imposed on real power output, which is then set to μS.

The inverter Volt-VAR function is also assumed present on the condition that it does not infringe on real power output, through a pre-defined limit on the maximum absolute reactive power, or by imposing a physical limit on the maximum apparent power. Note that as the traditional model of an inverter as having a limit on the apparent power output is derived from a nominal value of voltage with a current limit, it follows that in an overvoltage situation the capacity may be larger than the nominal amount.

By limiting the maximum amount of reactive power output $Q_{\lim} > 0$ admissible to the grid (typically defined in terms of a minimum power factor at maximum capacity) and combining this constraint with the physical limitations of the inverter, the maximum absolute amount of reactive power that can be injected by the inverter is

$$Q_{ma} = \min\left\{Q_{\lim}, \sqrt{S^2 - \mathcal{P}(E)^2}\right\} \leq S. \tag{9}$$

The Volt-VAR function $\mathcal{Q}(E)$ specifies the amount of VARs to be injected as a dynamic function of Q_{ma}, which fluctuates as a function of $\mathcal{P}(E)$. We define $\mathcal{Q}(E)$ as

$$\mathcal{Q}(E) = \begin{cases} 0 & \text{if } E < E_C, \\ -Q_{ma}\frac{E-E_C}{E_D-E_C} & \text{if } E \in [E_C, E_D], \\ -Q_{ma} & \text{if } E > E_D. \end{cases} \tag{10}$$

The definition of $\mathcal{Q}(E)$ in (10) prioritises real power output over the provision of reactive power [18], since real power output is curtailed only after the injected reactive power has reached its maximum. Such priority is commonly recommended [8], [13], [27].

C. Voltage region of operation (control region)

The analysis that follows focuses on the case where the Volt-Watt and Volt-VAR functions (8) and (10) are configured so that the voltage E is in the region $\{E : E \in [E_A, E_B]$ and $E \geq E_D\}$, where both real power curtailment and reactive power injection functions are simultaneously in operation.

In the sequel we assume that the fractional real power μ available to the inverter for export is constant and sufficiently large, such that $\mu_{\lim} \leq \mu \leq 1$, where the lower bound

$$\mu_{\lim} \doteq \sqrt{1 - Q_{\lim}^2/S^2} \tag{11}$$

is defined by the maximum admissible reactive power injection level $Q_{\lim} \in (0, S]$. This means that the inverter operates at maximum capacity within the voltage region of operation of interest $[E_A, E_B]$, namely,

$$\mathcal{P}(E)^2 + \mathcal{Q}(E)^2 = S^2, \tag{12}$$

which in turn implies that E_k does not exceed the value

$$E_{\lim} = E_A + \frac{1}{d}\left(1 - \frac{\mu_{\lim}}{\mu}\right). \tag{13}$$

Note that $\mu_{\lim}$ represents the limit value of power factor consistent with the maximum admissible level of reactive power injection $Q_{\lim}$.

Summarising the assumptions above, in the voltage region of interest (8), (10) and (12) reduce to

$$\boxed{\begin{aligned} \mathcal{P}(E) &= \mu S\left(1 - d(E - E_A)\right), \\ \mathcal{Q}(E) &= -\sqrt{S^2 - \mathcal{P}(E)^2}, \\ \mu &\in [\mu_{\lim}, 1], \\ E_k &\in [E_A, E_{\lim}]. \end{aligned}} \tag{14}$$

The voltage region of operation considered is illustrated in Figure 3 in terms of $\mathcal{P}(E)$ and $\mathcal{Q}(E)$.

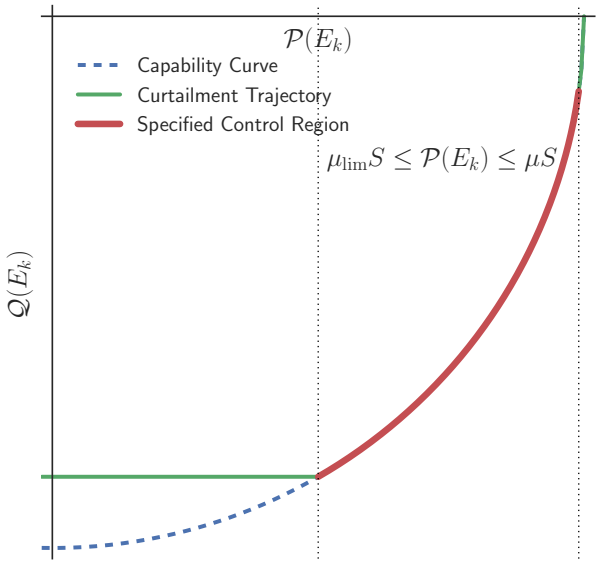

Fig. 3. The operating voltage region under study (control region).

III. Voltage dynamics under simultaneous operation of the Volt-Watt and Volt-VAR response functions

A. System dynamics and nonlinearities

Following a practise common in recent analyses of inverter microgrids [28], [29] and industry standards [10, p. 18], all delays and dynamics arising in the measurement of voltage E_k and the computation of the inverter power outputs $\mathcal{P}(E_k), \mathcal{Q}(E_k)$ are lumped in a simple discrete-time low-pass filter model of the form

$$E_{k+1} = aE_k + (1 - a)\,U_k, \tag{15}$$

where $0 \leq a < 1$ and the input U_k represents the inverter bus voltage U sampled at time k.

The voltage measurement dynamics (15) are assumed to be much slower than the electric transients arising in the line when the inverter outputs $P = \mathcal{P}(E_k)$ and $Q = \mathcal{Q}(E_k)$ are adjusted at the arrival of each voltage measurement sample E_k. Therefore, U_k is taken as the steady-state high-voltage feasible solution U^+ of the power flow equation (1) obtained using (6) with $P = \mathcal{P}(E_k)$ and $Q = \mathcal{Q}(E_k)$. We write the

resulting dependency of U_k on the measure voltage E_k in compact form as

$$U_k = F(E_k), \tag{16}$$

where the function F is defined from (6) as

$$F(E) \doteq \sqrt{G(E) + {}^{V^2}\!/_2 + H(E)}, \tag{17}$$

with the functions G and H defined as

$$G(E) \doteq R\mathcal{P}(E) + X\mathcal{Q}(E), \tag{18}$$

$$H(E) \doteq \sqrt{\left(G(E) + {}^{V^2}\!/_2\right)^2 - S^2Z^2}. \tag{19}$$

The following properties of the functions $G(E)$ and $F(E)$ will be required to show the existence of an equilibrium in the voltage region of operation considered.

Lemma 2 (Monotonicity of $G(E)$ and $F(E)$)**.** *Under the assumptions* (14)*, given* $E \in [E_A, E_{\lim}]$*,*

(a) $G(E)$ is a convex and monotonically decreasing function.
(b) If $R\mu_{\lim}S - XS\sqrt{1-\mu_{\lim}^2} + V^2/2 > SZ$, then $F(E)$ is a real, positive and monotonically decreasing function.

Proof. (a) Under the conditions (14), and since $\mathcal{P}(E) \geq 0$, we have from (18) that the derivative

$$G'(E) = -\mu S d\left(R + \frac{X\mathcal{P}(E)}{\sqrt{S^2 - \mathcal{P}^2(E)}}\right) < 0,$$

which includes the case $\mu = 1$ by taking $\lim_{E\to E_A^+} G'(E) = -\infty$, and shows that $G(E)$ is decreasing. Moreover, since

$$G''(E) = \frac{\mu^2 S^4 d^2 X}{\left(S^2 - \mathcal{P}^2(E)\right)^{3/2}} > 0,$$

$G(E)$ is in fact convex in $[E_A, E_{\lim}]$.

(b) Since $G(E)$ is decreasing in $[E_A, E_{\lim}]$, it attains its minimum at $E = E_{\lim}$. This minimum may be expressed as

$$\min_{[E_A, E_{\lim}]} G(E) = G(E_{\lim}) = R\mu_{\lim}S - XS\sqrt{1-\mu_{\lim}^2}, \tag{20}$$

by substituting (13) in (18). The expression (20) with the condition $R\mu_{\lim}S - XS\sqrt{1-\mu_{\lim}^2} + V^2/2 > SZ$ imply that

$$G(E) + V^2/2 > SZ \Rightarrow (G(E) + V^2/2)^2 - S^2Z^2 > 0$$

for E in $[E_A, E_{\lim}]$, which shows that $H(E)$ in (19) is real and positive, and in consequence so is $F(E)$ in (17). Note that this condition implies (7) holds, and hence that the power flow equation (1) has real positive solutions.

By differentiating (17) with respect to E, it is seen that

$$F'(E) = \frac{G'(E)F(E)}{2H(E)} < 0, \tag{21}$$

since $F(E)$ and $H(E)$ are real and positive and $G'(E)$ is negative. This shows that $F(E)$ is also strictly decreasing in $[E_A, E_{\lim}]$. □

B. Existence of an equilibrium voltage

The following result establishes simple sufficient conditions under which the discrete-time system (15) has an equilibrium within $[E_A, E_{\lim}]$ where the Volt-Watt and Volt-VAR response functions are simultaneously active.

Proposition 3 (Existence of an equilibrium voltage)**.** *Consider the inverter system with dynamics* (15) *subject to the conditions* (14) *and the algebraic relationship* (1) *where P and Q are replaced by the Volt-Watt and Volt-VAR response functions defined in* (8) *and* (10)*. Under the condition of Lemma 2(b), then*

$$F(E_A) \geq E_A \quad \textit{and} \quad F(E_{\lim}) \leq E_{\lim}, \tag{22}$$

if and only if (15) *has a unique equilibrium $E = E^* \in [E_A, E_{\lim}]$ that satisfies equation* (1) *with $P = \mathcal{P}(E^*)$ and $Q = \mathcal{Q}(E^*)$.*

Proof. We first show that a unique equilibrium E^* exists in $[E_A, E_{\lim}]$ whenever (22) is satisfied.

Lemma 2 implies that $F(E)$ is continuous, real, positive and strictly monotonically decreasing in $[E_A, E_{\lim}]$. It then follows from the boundary conditions (22) and the intermediate value theorem (see, e.g. [30, Theorem 4.23]) that $F(E)$ has a unique fixed-point $E^* = F(E^*)$ in $[E_A, E_{\lim}]$. This fixed-point is an equilibrium of (15), since if $E_k = E^*$ at a time k, then at time $k+1$,

$$E_{k+1} = aE^* + (1-a)F(E^*) = E^*.$$

Direct substitution shows that $F(E^*) = E^*$ is indeed a solution of equation (1) when P and Q are substituted by $P = \mathcal{P}(E^*)$ and $Q = \mathcal{Q}(E^*)$.

To see that condition (22) is also necessary, suppose that there exist a voltage $E^* \in [E_A, E_{\lim}]$ such that $F(E^*) = E^*$. Then (22) follows from the fact that $F(E)$ is continuous and strictly monotonically decreasing in $[E_A, E_{\lim}]$, and thus, $F(E) \geq E$ for $E \leq E^*$, and $F(E) \leq E$ for $E \geq E^*$. □

The boundary conditions (22) may be alternatively checked using the algebraic expression on the left hand side of equation (1). Namely, $F(E_A) \geq E_A$ is equivalently mapped to

$$E_A^4 - \left(2(\mathcal{P}(E_A)R + \mathcal{Q}(E_A)X) + V^2\right)E_A^2 + S^2Z^2 \leq 0,$$

and $F(E_{\lim}) \leq E_{\lim}$ is equivalently mapped to

$$E_{\lim}^4 - \left(2(\mathcal{P}(E_{\lim})R + \mathcal{Q}(E_{\lim})X) + V^2\right)E_{\lim}^2 + S^2Z^2 \geq 0.$$

These equivalences may be verified by squaring the inequalities in (22) and completing squares to construct the double quadratic function on the left hand side of equation (1).

C. Computation of the equilibrium voltage

Obtaining an explicit analytic expression for the equilibrium voltage E^* is generally difficult. However, under the conditions (22), E^* may be numerically computed to any desired precision using the expression for F given in (17). Standard numerical procedures to find roots of a function can be applied to the function $F(E) - E$ to find $E^* : F(E^*) - E^* = 0$.

A bisection procedure to do so is illustrated in Algorithm 1. The bisection method is simple and its convergence to within

a given error tolerance ϵ is guaranteed, with an error that is halved at each iteration [31, Chapter 8]. A disadvantage of the bisection procedure is its relatively slow convergence.

Algorithm 1: Bisection procedure to compute equilibrium voltage E^* in $[E_A, E_{\lim}]$ to within error ϵ.

Data: parameters $E_A, E_{\lim}, R, X, V, S, d, \mu_{\lim}, \mu$, tolerance ϵ
Result: equilibrium voltage E^*

Check condition (22) in Proposition 3;
if $(F(E_A) - E_A)(F(E_{\lim}) - E_{\lim}) > 0$ **then**
  return *No equilibrium in* $[E_A, E_{\lim}]$

Initialisation;
$A \leftarrow E_A$;
$B \leftarrow E_{\lim}$;
$C \leftarrow (A + B)/2$;

Computation;
while $|F(C) - C| > \epsilon$ **do**
  if $((F(A) - A)(F(C) - C) < 0)$ **then**
    $B \leftarrow C$
  else
    $A \leftarrow C$
  $C \leftarrow (A + B)/2$;
$E^* \leftarrow C$

Alternatively, a faster procedure based on the Newton-Raphson method could be implemented using also the expression for F' in (26), as shown in Algorithm 2. The disadvantage of the Newton-Raphson procedure is that its convergence can only be guaranteed if its initial condition is a sufficiently close approximation to the sought root (see e.g. [31, Chapter 8]). However, a suitable initial condition may be obtained by running a few iterations of the bisection procedure in Algorithm 1, and then follow refinement via the Newton-Raphson procedure in Algorithm 2 to obtain a combined procedure with guaranteed convergence and improved convergence speed. For illustration, using the parameters listed in (28) E^* is computed to within $\epsilon = 10^{-6}$ in 23 iterations with Algorithm 1, and in 6 iterations with Algorithm 2 initialised with $E_0 = (E_A + E_{\lim})/2$.

We apply these algorithms to compute the system equilibria in the numerical studies in Section IV.

D. Stability of the equilibrium voltage

Assuming the Volt-Watt and Volt-VAR responses are instantaneously computed from the measured voltage E_k (all delays and dynamics in the loop are lumped in the dynamics of the voltage measurement filter (15)–(16)), then the stability of the interaction between these response functions around an equilibrium $E^* \in [E_A, E_{\lim}]$ is determined by the magnitude of the Jacobian of the difference equation (15),

$$\rho \doteq \left| \frac{\partial \left(aE + (1-a)F(E) \right)}{\partial E} \right|_{E=E^*} = |a + (1-a)F'(E^*)|. \quad (23)$$

Algorithm 2: Newton-Raphson procedure to compute equilibrium voltage E^* in $[E_A, E_{\lim}]$ to within error ϵ.

Data: parameters $E_A, E_{\lim}, R, X, V, S, d, \mu_{\lim}, \mu$, tolerance ϵ, initial condition $E_0 \in [E_A, E_{\lim}]$
Result: equilibrium voltage E^*

Check condition (22) in Proposition 3;
if $(F(E_A) - E_A)(F(E_{\lim}) - E_{\lim}) > 0$ **then**
  return *No equilibrium in* $[E_A, E_{\lim}]$

Initialisation;
$C \leftarrow E_0$;

Computation;
while $|F(C) - C| > \epsilon$ **do**
  $C \leftarrow C - \dfrac{F(C) - C}{F'(C) - 1}$
$E^* \leftarrow C$

Discrete-time system stability theory establishes that the equilibrium of the system will be exponentially stable if and only if $\rho = |a + (1-a)F'(E^*)| < 1$ (see for example [32, Theorem 22.11]). This result may be translated from (23) into the following tests for stability and instability.

Proposition 4 (Theoretic tests for stability)**.** *Assume the conditions of Proposition 3 are satisfied. Then*

(T1) The equilibrium E^* of system (15) *is locally exponentially stable if and only if*

$$F'(E^*) + \frac{1+a}{1-a} > 0.$$

(T2) The equilibrium E^* is unstable if

$$F'(E^*) + \frac{1+a}{1-a} < 0.$$

Proof. The expressions follow directly from (23) and application of Theorem 22.11 in [32] and the fact that $F'(E) < 0$ for E in $[E_A, E_{\lim}]$. □

The case of $F'(E^*) + (1+a)/(1-a) = 0$, not considered in Proposition 4, corresponds to the Jacobian of the system having an eigenvalue on the boundary of the stability region. The stability of this singular point requires more advanced analysis (e.g. [33, Chapter 8]) beyond the scope of the paper.

While Proposition 4 provides non-conservative tests for stability, they require the knowledge of the equilibrium voltage E^*, which is hard to characterise analytically, as discussed in Section III-C. However, these theoretic tests may be used by computing E^* for a given set of system parameters using Algorithms 1 and 2, as illustrated in Section IV-B.

To obtain stability tests that do not require computation of E^*, we derive from (T1) and (T2) sufficient analytic conditions for stability and instability as explicit expressions of the system parameters. These sufficient conditions help to evaluate the impact of these parameters on stability without numerical computations, at the expense of some conservativeness.

Corollary 5 (Parametric tests for stability)**.** *Under the conditions of Proposition 3,*

(P1) The equilibrium E^* of system (15) *is locally exponentially stable if*

$$-\mu Sd\left(R+\frac{X\mu}{\sqrt{1-\mu^2}}\right)\frac{E_{\lim}}{2H(E_{\lim})}+\frac{1+a}{1-a}>0. \quad (24)$$

(P2) The equilibrium E^* is unstable if

$$-\mu Sd\left(R+\frac{X\mu_{\lim}}{\sqrt{1-\mu_{\lim}^2}}\right)\frac{E_A}{2H(E_A)}+\frac{1+a}{1-a}<0. \quad (25)$$

Proof. Expression (21) and the facts that $E_A \le E^* = F(E^*) \le E_{\lim}$, and that $G(E) > 0$ is monotonically decreasing (and so is then $H(E) > 0$), and $G'(E) < 0$ is monotonically increasing in $[E_A, E_{\lim}]$ (since $G(E)$ is convex), yield the bounds

$$F'(E^*) = \frac{G'(E^*)E^*}{2H(E^*)} \ge \frac{G'(E_A)E_{\lim}}{2H(E_{\lim})}, \quad (26)$$

$$F'(E^*) = \frac{G'(E^*)E^*}{2H(E^*)} \le \frac{G'(E_{\lim})E_A}{2H(E_A)}. \quad (27)$$

Then, (26) and (T1) leads to (P1), and (27) and (T2) to (P2) after substituting $G'(E_A) = \mu Sd\big(R + X\mu/\sqrt{1-\mu^2}\big)$ and $G'(E_{\lim}) = \mu Sd\big(R + X\mu_{\lim}/\sqrt{1-\mu_{\lim}^2}\big)$. □

In comparison with Proposition 4, the tests in Corollary 5 are conservative, in the sense that if their conditions are not satisfied one cannot conclude stability or instability of the equilibrium. However, the tests in Corollary 5 permit direct analytic evaluation of the impact on stability of line and inverter parameters, such as the ratio X/R, the droop gain d, and the voltage measurement filter parameter a.

The parametric test (P1) may be used as a means to draw design guidelines for safe parameter ranges that guarantee exponentially stable equilibria over the voltage region of operation, without need for precise equilibrium voltage calculations.

E. Analytic implications

Corollary 5(P2) shows that unstable interactions between the Volt-Watt and Volt-VAR inverter response functions are indeed possible when the inverter operates near capacity if real power output takes precedence over the provision of reactive power. Note that this observation places a caveat on a typically suggested setting for inverters that aims to maximise injected active power [8], [13], [27]. As shown by the above results, insisting on maximal active power injection introduces a potential instability risk when the inverter is at capacity, by a mechanism that first unintentionally restricts reactive power output in the Volt-VAR droop range, and then reenables it once the voltage reaches the Volt-Watt droop range.

The explicit dependence of the equilibrium stability on the impedance of the line and the voltage measurement filter captured by the tests (P1) and (P2) are in correspondence with observations made in [13], [14]. Indeed, note how the stability margin of the equilibrium is reduced as the filter is made faster as $a \to 0$. Namely, the condition (24) for exponential stability is less likely to be satisfied, and the condition (25) for instability is more likely to be satisfied for a given set of system parameters. On the other hand, these analytic conditions also show that for any given set of line and inverter parameters, the equilibrium can always be made stable by making the filter sufficiently slow, as $a \to 1$.

The influence of the bandwidth of the voltage measurement filter on the stability of these automatic response mechanisms to mitigate overvoltages has been observed in [14] and [13]. In [14] it is noted that a voltage measurement filter with sufficient damping is required for the voltage controller to find a new steady operation point after perturbation in a system comprising two parallel inverters with Volt-VAR and Volt-Watt automatic response functions.

In [13] the stability of a system where only a Volt-VAR response function is active is shown to have instances where a fast filter with $a = 0$ (referred to as Type-A in [13]) leads to instability, while a slower filter with $a = 0.9$ (referred to as Type-B in [13]) leads to a stable system. Note, however, that even in the latter case instability may arise in the interaction between Volt-VAR and Volt-Watt responses, as may be seen from (P2) if, for example, the X/R ratio is sufficiently high. This point is illustrated in the numerical study in Section IV-B.

Sensitivity to other system parameters can also be studied from (24) and (25). The active power droop gain d, for example, reduces the stability margin of the system as d is increased. For inductive lines, instability is more likely when the maximum admissible level of reactive power $Q_{\lim}$ is lower, which makes $\mu_{\lim} \to 1$, as can be seen from (11). The latter is emphasised for lines that are more predominantly inductive, namely, lines with higher X/R ratio.

IV. Numerical studies

A. Simulation example

An illustrative two-bus system featuring an inverter and a voltage source (Figure 2) was simulated in PYPOWER, an open source port of MATPOWER [34] developed in the Python programming language. For each timestep, the measured voltage (E_{k+1} in (15)) was calculated using the voltage value U_k returned from the load flow calculation (substituted for $F(E_k)$) and the previous measured value (E_k). The resultant value for E_{k+1} was then used to calculate the appropriate amount of real and reactive power output from the inverter for the next time step.

A realistic scenario was simulated using the parameters

$$\begin{aligned} E_A &= 240\text{V}, & E_B &= 250\text{V}, & V &= 230\text{V}, \\ R &= 0.606\Omega, & X &= 1.251\Omega, & S &= 10\text{kVA}, \\ d &= 10\%\text{/V}, & \mu_{\lim} &= 0.95, & \mu &= 0.99. \end{aligned} \quad (28)$$

For these parameters, Lemma 2(b) is satisfied because

$$\frac{R}{Z}\mu_{\lim} - \frac{X}{Z}\sqrt{1-\mu_{\lim}^2} + \frac{V^2}{2SZ} = 2.036 > 1.$$

The inequalities in (22) are satisfied with $F(E_A) = 240.91\text{V} \ge E_A = 240\text{V}$ and $F(E_{\lim}) = 230.11\text{V} \le E_{\lim} = 240.40\text{V}$, which by Proposition 3 guarantee the existence of an equilibrium $E^* \in [E_A, E_{\lim}]$.

The equilibrium voltage E^* was numerically found to be $240.023\,V$, which gives $F'(E^*) = -37.31$. As Figure 4 and 5 show, using $a = 0.90$ or $a = 0.94$ in the filter makes this

equilibrium unstable, while $a = 0.96$ makes it exponentially stable. This is predicted by the theoretic tests in Proposition 4,

$$\left.\begin{aligned} F'(E^*) + \tfrac{1+a}{1-a}\big|_{a=0.90} &= -18.31 \\ F'(E^*) + \tfrac{1+a}{1-a}\big|_{a=0.94} &= -4.98 \end{aligned}\right\} \Rightarrow \text{instability by (T2)},$$
$$F'(E^*) + \tfrac{1+a}{1-a}\big|_{a=0.96} = 11.68 \quad \Rightarrow \text{stability by (T1)}.$$

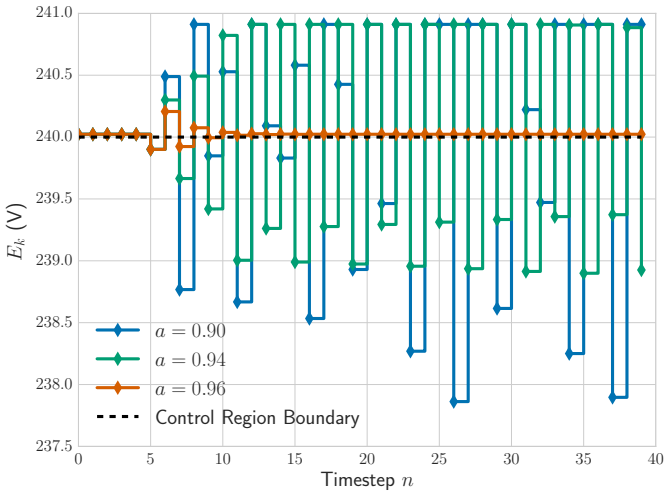

Fig. 4. Time-domain response of the voltage E_k at the point of connection of the inverter to the line. The responses are unstable for $a = 0.90$ and $a = 0.94$, and exponentially stable for $a = 0.96$. The lower end of the control region (240V) is indicated in dash line. The equilibrium voltage in this case, $E^* = 240.023$ is the limiting value of the exponentially stable response obtained for $a = 0.96$.

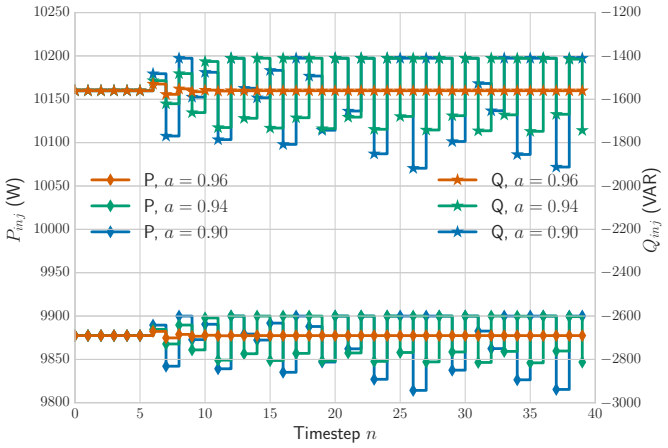

Fig. 5. Time-domain responses of the inverter output active and reactive powers $\mathcal{P}(E_k)$ (left vertical axis) and $\mathcal{Q}(E_k)$ (right vertical axis) for different values of the voltage measurement filter parameter a. The responses are unstable for $a = 0.90$ and $a = 0.94$, and exponentially stable for $a = 0.96$.

The evaluation of the left hand sides of the bounds given by Corollary 5 yields

$$\begin{aligned} \text{LHS of (25)}\big|_{a=0.90} &= -0.14 \;\; < 0 \Rightarrow \text{instability by (P2)}, \\ \text{LHS of (25)}\big|_{a=0.94} &= 13.19 \;\; > 0 \quad \text{(P2) inconclusive}, \\ \text{LHS of (24)}\big|_{a=0.94} &= -12.92 < 0 \quad \text{(P1) inconclusive}, \\ \text{LHS of (24)}\big|_{a=0.96} &= 3.74 \;\; > 0 \Rightarrow \text{stability by (P1)}. \end{aligned}$$

The bound given by (P2) implies instability for values of $a \leq 0.9001$, while the theoretical test (T2) implies instability for values of $a \leq 0.9522$, which illustrates the degree of conservativeness of the parametric tests in Corollary 5. Further comparison between the theoretical and parametric tests for stability is provided in the next numerical study, which maps stability regions over the parameter space spanned by a and the ratio X/R.

B. Stability margins with respect to line impedance and voltage measurement filter

A numerical sensitivity study was conducted to analyse stability of the equilibrium voltage E^* with respect to the line impedance X/R ratio, and the voltage measurement filter bandwidth parameter a. The system considered is defined by the nominal parameters listed in (28), except for

- R and X, which are varied, such that X/R ranges over 500 values distributed in the interval $[1.4, 2.15]$ that satisfy the constraint $X + R = 1.875$ (satisfied by the nominal values of X and R listed in (28)), and
- a, which is varied, ranging over 500 values distributed in the interval $[0.85, 1]$.

For each of the 500×500 pairs $\{X/R, a\}$ sampled from their ranges, the resulting equilibrium voltage E^* is numerically computed to within a precision of $\epsilon = 10^{-4}$ by means of a procedure that combines the bisection method in Algorithm 1 and the Newton-Raphson method in Algorithm 2 to guarantee convergence and improve convergence speed. The chosen ranges for X/R and a are such that the conditions of Proposition 3 are satisfied for every combination and thus the ensuing equilibria E^* are in $[E_a, E_{\lim}]$.

The conditions from Proposition 4 and Corollary 5 were evaluated at each equilibrium voltage E^* to determine exponential stability or instability. Figure 6 maps the stability regions obtained over the range of values of X/R and a.

The map is divided into top and bottom halves by a curve in solid line that represents the theoretical stability boundary corresponding to the tests (T1) and (T2), namely

$$F'(E^*) + \frac{1+a}{1-a} = 0.$$

The top half (light and dark grey) above the theoretical stability boundary corresponds to exponentially stable equilibria, while the botom half (light and dark green) below the theoretical stability boundary represents unstable equilibria.

Each of these halves is in turn divided by curves in dotted lines. These curves represent the stability boundary for which the parametric tests (P1) (top dotted line) and (P2) (bottom dotted line) are conclusive. The darker grey area at the top of the stable region represents stable equilibria implied by (P1). Similarly, the darker area at the bottom of the instability region represents unstable equilibria as implied by (P2).

Note that the degree of conservatism of (P1) and (P2) with respect to (T1) and (T2) is quantified by the extent of the lighter (grey and green) areas. Observe how the stability test (P1) is less conservative for lower values of X/R and a, while in contrast, the instability test (P2) becomes less conservative for higher values of X/R and a.

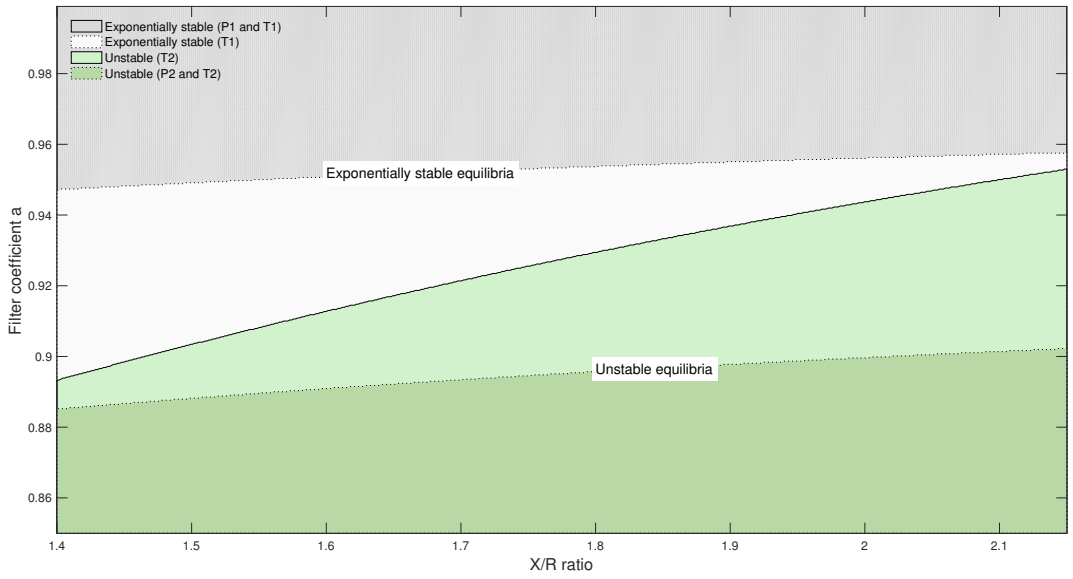

Fig. 6. Theoretic and parametric stability regions as functions of the X/R ratio and the filter coefficient a. The same parameters as listed in (28) apply, with the exception of X, R, which are varied such that $X + R = 1.857$ $(= 1.251 + 0.606)$ remains constant.

In correspondence with our analytic observations in Section III-E, line impedances with higher values of X/R (more inductive) show reduced margins of stability, which are further reduced by relatively smaller measurement filter coefficient values a (faster voltage measurement).

V. Conclusions

This paper has presented a rigorous stability analysis of a grid-connected inverter under simultaneous operation of automatic Volt-Watt and Volt-VAR response functions to mitigate overvoltage issues. The inverter is assumed to be a current-controlled inverter operating at or near capacity in real power output, which is assumed to take precedence over the production of reactive power, as recommended in current standards and guidelines [8], [9].

The analysis presented by the paper provides sufficient conditions for the existence of an equilibrium in the voltage region of simultaneous operation of the Volt-Watt and Volt-VAR response functions. The stability of this equilibrium is determined by theoretical and parametric stability tests, which may be evaluated numerically or analytically. The parametric tests are useful to analytically identify safe parameter ranges for design implementation with guaranteed stability margins. The paper discussed implications of these tests on how stability is affected by key system parameters, such as the inverter voltage measurement filter bandwidth, Volt-Watt droop response gain, maximum admissible level of reactive power, and line impedance X/R ratio. The observed impact of these parameters is consistent with previous stability studies for inverters with Volt-VAR response function [13], [16].

An important observation derived from the analysis is the existence of an inherent stability vulnerability in the interaction between Volt-Watt and Volt-VAR inverter response functions, which appears not to have been identified previously. This vulnerability arises under a typically recommended inverter design configuration, where real power output takes precedence over the absorption of VARs for voltage support.

Fundamentally, the stability vulnerability identified is caused by the fact that the Volt-VAR support in the instance of overvoltage is inhibited by the inverter being at or near its capacity limit for real power output, which is given precedence over the production of reactive power output. While VAR support is triggered for voltages $E > E_C$, VAR injection may be constrained if there is sufficiently high real power output. If the voltage then rises to E_A, real power output is curtailed alongside increased VAR injection, potentially causing high rates of change of voltage and real/reactive power, due to the quadratic coupling (12) between active and reactive power outputs. This vulnerability does not exist if the precedence of the Volt-Watt and Volt-VAR response functions is changed by adopting a "reactive power preferred" model [18].

By setting precedence on reactive power, additional real power losses will occur, which may not be a desirable solution to PV owners. However, this has been argued to be of minor practical consequence [18]. In this case, it is necessary to bound the maximum absolute reactive power injected by the inverter to avoid similar stability issues that can potentially exist, due to an arbitrarily large negative gradient if $E_D \leq E_B$. Alternatively, stability margins may be increased while preserving the real power preferred model by careful adjustment of the system parameters to guarantee that the sufficient condition for exponential stability prescribed by the proposed stability criteria (Corollary 5(P1)) is satisfied.

Voltage-controlled inverters, connected to the grid as voltage sources rather than as current sources, may be more suitable

to feed power to the grid under high levels of renewable energy penetration [35]. Voltage-controlled inverters naturally regulate voltage and may be configured to mimic conventional synchronous generators to directly participate in the regulation of power system frequency and voltage via well-established droop-control techniques [4, Chapter 18].

While the analysis presented applies to any grid-connected current-controlled inverter irrespective of the larger network configuration, it is limited to internal loop dynamics involving the voltage measured at the inverter point of connection. The stability analysis of dynamic interactions across multiple inverters is a subject of ongoing research.

Acknowledgement

The authors gratefully acknowledge funding from ARENA, the Australian Renewable Energy Agency under Grant No. 2014/RND032. The views expressed herein are the authors' and not necessarily the views of the Australian Government, and the Australian Government does not accept responsibility for any information or advice contained herein.

References

[1] H. Wirth, "Recent facts about photovoltaics in Germany," Fraunhofer Institute for Solar Energy Systems ISE, Tech. Rep., April 2016.

[2] APVI, "Solar map," 2016. [Online]. Available: http://pv-map.apvi.org.au

[3] C. E. Regulator, "Postcode data for small-scale installations," 2017. [Online]. Available: http://www.cleanenergyregulator.gov.au/RET/Forms-and-resources/Postcode-data-for-small-scale-installations

[4] Q.-C. Zhong and T. Hornik, *Control of power inverters in renewable energy and smart grid integration*. John Wiley & Sons, Ltd, 2013.

[5] S. Sayeef, S. Heslop, D. Cornforth, T. Moore, S. Percy, J. K. Ward, A. Berry, and D. Rowe, "Solar intermittency: Australia's clean energy challenge," CSIRO, Tech. Rep., 2012. [Online]. Available: https://publications.csiro.au/rpr/download?pid=csiro:EP121914&dsid=DS1

[6] Ergon Energy and Energex, "Connection standard: Small scale parallel inverter energy systems up to 30 kVA," Ergon Energy and Energex, Tech. Rep. EX BMS4286 V.2, 2014.

[7] Horizon Power, "Technical requirements for renewable energy systems connected to the low voltage (LV) network via inverters," Horizon Power, Tech. Rep. HPC-9FJ-12-0001-2012, 2014.

[8] EPRI, "Common Functions for Smart Inverters, Version 3," EPRI, Palo Alto, CA, USA, Tech. Rep. 3002002233, 2013.

[9] Standards Australia, "AS/NZS 4777.2:2015 Grid connection of energy systems via inverters Part 2: Inverter requirements," Oct. 2015.

[10] NEN, "European standard NEN-EN 50438: Requirements for micro-generating plants to be connected in parallel with public low-voltage distribution networks," Dec. 2013.

[11] EPRI, "Advanced grid support functions for smart inverters. Toward a unified regulatory framework in europe," Electric Power Research Institute, Palo Alto, CA, USA, Technical Update report, 11 2016.

[12] E. Demirok, D. Sera, R. Teodorescu, P. Rodriguez, and U. Borup, "Evaluation of the voltage support strategies for the low voltage grid connected pv generators," in *Proceedings of the 2010 IEEE Energy Conversion Congress and Exposition, ECCE 2010*, 2010, pp. 710–717.

[13] P. Jahangiri and D. Aliprantis, "Distributed Volt/VAR control by PV inverters," *IEEE Transactions on Power Systems*, vol. 28, no. 3, pp. 3429–3439, 2013.

[14] T. Stetz, "Autonomous Voltage Control Strategies in Distribution Grids with Photovoltaic Systems: Technical and Economical Assessment," Ph.D. dissertation, University of Kassel, Kassel, Nov. 2013.

[15] S. Weckx, C. Gonzalez, and J. Driesen, "Combined central and local active and reactive power control of pv inverters," *IEEE Transactions on Sustainable Energy*, vol. 5, no. 3, pp. 776–784, 2014.

[16] F. Andrén, B. Bletterie, S. Kadam, P. Kotsampopoulos, and C. Bucher, "On the stability of local voltage control in distribution networks with a high penetration of inverter-based generation," *IEEE Transactions on Industrial Electronics*, vol. 62, no. 4, pp. 2519–2529, 2015.

[17] R. Tonkoski, L. Lopes, and T. El-Fouly, "Coordinated active power curtailment of grid connected pv inverters for overvoltage prevention," *IEEE Transactions on Sustainable Energy*, vol. 2, no. 2, pp. 139–147, 2011.

[18] L. Collins and J. K. Ward, "Real and reactive power control of distributed PV inverters for overvoltage prevention and increased renewable generation hosting capacity," *Renewable Energy*, vol. 81, pp. 464–471, Sep. 2015.

[19] M. Ghasemi and M. Parniani, "Prevention of distribution network overvoltage by adaptive droop-based active and reactive power control of pv systems," *Electric Power Systems Research*, vol. 133, pp. 313–327, 2016.

[20] S. Pukhrem, M. Basu, M. Conlon, and K. Sunderland, "Enhanced network voltage management techniques under the proliferation of rooftop solar pv installation in low voltage distribution network," *IEEE Journal of Emerging and Selected Topics in Power Electronics*, vol. PP, no. 99, pp. 1–1, 2016, early Access Article.

[21] K. Baker, A. Bernstein, E. Dall'Anese, and C. Zhao, "Network-Cognizant Voltage Droop Control for Distribution Grids," *ArXiv e-prints*, Feb. 2017. [Online]. Available: https://arxiv.org/abs/1702.02969

[22] P. Kundur, *Power system stability and control*. McGraw-Hill, 1994.

[23] J. H. Braslavsky, J. K. Ward, and L. Collins, "A stability vulnerability in the interaction between Volt-VAR and Volt-Watt response functions for smart inverters." in *Proc. of the 2015 IEEE Conference on Control Applications (CCA)*, Sydney, Australia, Sep. 2015, pp. 733–738.

[24] J. D. Glover, M. S. Sarma, and T. J. Overbye, *Power system analysis and design, 5/e, SI edition*, 5th ed. Stamford, CT: South-Western, Cengage Learning, 2011.

[25] H.-D. Chiang and M. Baran, "On the existence and uniqueness of load flow solution for radial distribution power networks," *IEEE Transactions on Circuits and Systems*, vol. 37, no. 3, pp. 410–416, 1990.

[26] B. Venkatesh, R. Ranjan, and H. Gooi, "Optimal reconfiguration of radial distribution systems to maximize loadability," *IEEE Transactions on Power Systems*, vol. 19, no. 1, pp. 260–266, 2004.

[27] K. Turitsyn, P. Sulc, S. Backhaus, and M. Chertkov, "Distributed control of reactive power flow in a radial distribution circuit with high photovoltaic penetration," in *Proceedings of the IEEE PES General Meeting, PES 2010*, 2010.

[28] J. Schiffer, R. Ortega, A. Astolfi, J. Raisch, and T. Sezi, "Conditions for stability of droop-controlled inverter-based microgrids," *Automatica*, vol. 50, no. 10, pp. 2457–2469, 2014.

[29] J. Simpson-Porco, Q. Shafiee, F. Dorfler, J. Vasquez, J. Guerrero, and F. Bullo, "Secondary frequency and voltage control of islanded microgrids via distributed averaging," *IEEE Transactions on Industrial Electronics*, vol. 62, no. 11, pp. 7025–7038, 2015.

[30] W. Rudin, *Principles of mathematical analysis*, 3rd ed. McGraw-Hill, 1976.

[31] G. Phillips and P. Taylor, *Theory and Applications of Numerical Analysis*, 2nd ed. Academic Press, 2007.

[32] W. J. Rugh, *Linear system theory*, 2nd ed. Prentice Hall, 1996.

[33] H. K. Khalil, *Nonlinear systems*, 3rd ed. Prentice Hall, 2002.

[34] R. D. Zimmerman, C. E. Murillo-Sanchez, and R. J. Thomas, "MATPOWER: steady-state operations, planning and analysis tools for power systems research and education," *IEEE Transactions on Power Systems*, vol. 26, no. 1, pp. 12–19, 2011.

[35] J. C. Vasquez, R. A. Mastromauro, J. M. Guerrero, and M. Liserre, "Voltage support provided by a droop-controlled multifunctional inverter," *IEEE Transactions on Industrial Electronics*, vol. 56, no. 11, pp. 4510–4519, 11 2009.

Julio H. Braslavsky (M'99–SM'13) graduated as Electronic Engineer from the National University of Rosario, Argentina, in 1989, and received the Ph.D. degree from the University of Newcastle, Australia, in 1996. He is a Senior Research Scientist with the Grids and Energy Efficienty Systems research program at the Australian CSIRO, where he leads research to optimise the integration of renewable electricity generation and energy storage in low-voltage electricity grids. He is Conjoint Senior Lecturer at the School of Electrical Engineering and Computing at the University of Newcastle, and serves as Associate Editor for the IEEE TRANSACTIONS ON CONTROL SYSTEMS TECHNOLOGY. His research interests include modelling, estimation and control of electric load ensembles and distributed generation, and stability analysis of switched and sampled-data control systems.

Lyle D. Collins received the B. Engineering with 1st Class Honours (Electrical) and B. Science with Distinction (Photonics) degrees from the University of Newcastle, Callaghan, Australia, in 2013. He is a Research Technician at the CSIRO Energy Centre in Newcastle, Australia and currently working towards a Ph.D. degree in electrical engineering at the University of Newcastle and the CSIRO Energy Centre. His research interests include game theory, automated distributed systems, distribution electrical power systems and demand management. Mr. Collins was awarded the Engineers Australia Undergraduate Thesis Prize in 2013.

John K. Ward (M'04) graduated as Electrical Engineer (Hons I) from the University of Newcastle, Australia, in 1997 and with a Ph.D. in control theory in 2002. He is the Science Director of the Grids and Energy Efficiency Systems research program at the Australian CSIRO, with the responsibility of driving the program's science direction. He has contributed significantly to the development of Australian standards for demand response and distributed generation (AS/NZ4755 and AS/NZ4777). His research is focused on adding intelligence to the interaction of energy systems within electricity distribution networks — including energy efficient building systems, optimisation methods for distributed (energy) systems and multi-agent learning methods.